THE JOURNAL OF PHYSICAL CHEMISTRY A

ARTICLE

pubs.acs.org/JPCA

# Modeling Nonaqueous Proton Wires Built from Helical Peptides: Biased Proton Transfer Driven by Helical Dipoles

Gustavo E. López,*[,†,‡] Inara Colón-Díaz,[†] Anthony Cruz,[†,‡] Sumana Ghosh,[§] Samantha B. Nicholls,[§] Usha Viswanathan,[§] Jeanne A. Hardy,[§] and Scott M. Auerbach[§]

[†]Department of Chemistry, University of Puerto Rico at Mayagüez, Mayagüez, Puerto Rico 00681

[‡]Department of Chemistry, Lehman College-CUNY, Bronx, New York 10034, United States

[§]Department of Chemistry, University of Massachusetts at Amherst, Amherst, Massachusetts 01003, United States

**ABSTRACT:**

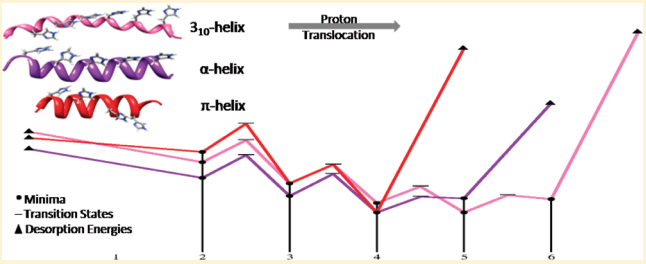


We report gas-phase electronic structure calculations on helical peptides that act as scaffolds for imidazole-based hydrogen-bonding networks (proton wires). We have modeled various 21-residue polyalanine peptides substituted at regular intervals with histidines (imidazole-bearing amino acids), using a hybrid approach with a semiempirical method (AM1) for peptide scaffolds and density functional theory (B3LYP) for proton wires. We have computed energy landscapes including barriers for Grotthuss-shuttling-type proton motions though wires supported on $3_{10}$-, $\alpha$- and $\pi$-helical structures, showing the $3_{10}$- and $\alpha$-helices to be attractive targets in terms of high proton affinities, low Grotthuss shuttling barriers, and high stabilities. Moreover, bias forces provided by the helical dipole moments were found to promote unidirectional proton translocation.

## I. INTRODUCTION

The promise of hydrogen-based energy has generated renewed interest in rationally designed proton exchange membranes that can function in hydrogen fuel cells.[1] Ideal properties for new proton exchange membrane materials include the ability to function through nonsolvent-mediated mechanisms, thus avoiding the problem of dehydration due to electro-osmotic drag. Some promising new proton exchange membrane materials use tethered imidazoles as the primary proton translocating functionality.[2] Because imidazoles can both donate and accept hydrogen bonds, they are capable of forming extended hydrogen-bonding networks, i.e., proton wires that act as proton transporters through the Grotthuss shuttling mechanism. Imidazoles are also used as proton translocating moieties in a number of native biological systems, inspiring biomimetic applications for this functional group.[3,4] Our previous calculations on nonpeptide proton wires show that backbone repeat distances in the range of 5−6 Å are required for continuous hydrogen-bond networks of imidazoles and triazoles, making helical peptides excellent candidates for such scaffolds.[5] In addition to their geometrical properties, helical peptides exhibit electric dipoles that may promote unidirectional proton motion. In this article, we report electronic structure calculations on helical-peptide-based proton wires, predicting for the first time the utility of these systems for solvent-free proton conduction.

Three major helical conformations of polypeptide chains can be formed from $\alpha$-amino acids: $3_{10}$-, $\alpha$-, and $\pi$-helices (Figure 1). In the present study, we consider 21-residue peptides with $3_{10}$-, $\alpha$-, and $\pi$-helical structures substituted with histidine (an imidazole-bearing amino acid) at regular intervals so that all imidazoles decorate a single face of the helix. In particular, we have examined the designed $3_{10}$-, $\alpha$-, and $\pi$-helical sequences $Ala_3(His\text{-}Ala_2)_6$, $Ala_2(His\text{-}Ala_3)_4HisAla_2$, and $Ala_2(His\text{-}Ala_4)_3HisAla_3$, respectively, using starting conformations of idealized $3_{10}$-, $\alpha$-, and $\pi$-structures. These particular peptide sequences were designed as polyalanine-substituted scaffolds because polyalanine has been well studied from both theoretical and experimental perspectives.[6−12] In particular, recent experimental studies[13,14] have shown that $\alpha$-helical polyalanine peptides are stable due to enthalpic factors that include cooperative H-bonding. The propensity of the helical conformation depends strongly on the terminal caps, length of the peptide, and temperature. These stabilization effects have been corroborated by electronic structure calculations.[15,16]

Within the concept of a proton wire, the helices can be viewed as having two distinct regions: one consists of all the alanine residues plus the C-$\alpha$ atoms of the histidine backbone (denoted

**Received:** October 24, 2011
**Revised:** December 19, 2011
**Published:** December 21, 2011

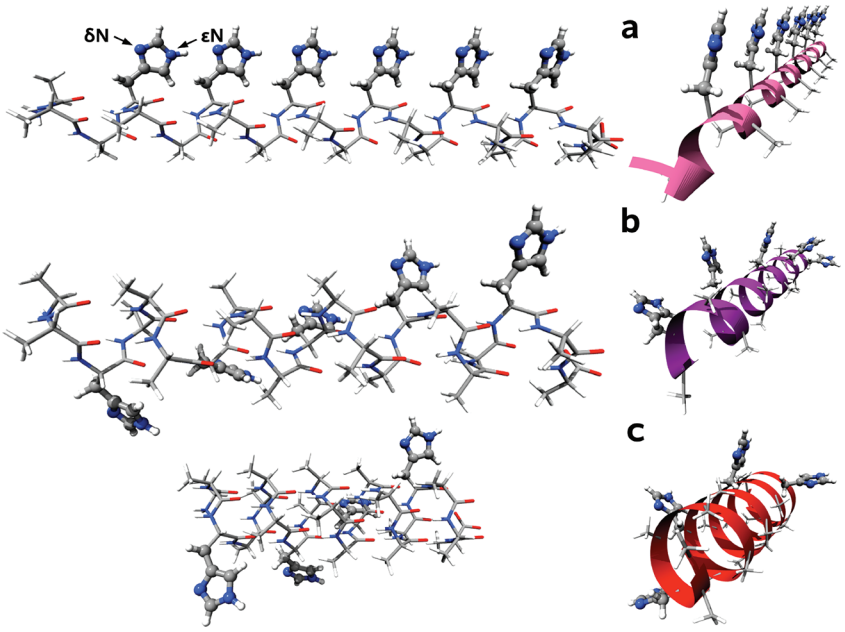


**Figure 1.** Initial structures of helical peptides illustrating geometrical differences between (a) $3_{10}$-helix, (b) $\alpha$-helix and (c) $\pi$-helix. Structures were generated based upon idealized models. Side-chain positions were added with Chimera software and are rendered from two different perspectives as all-atom stick model (left) and a ribbon backbone trace with only histidine side-chains shown in ball-and-stick (right). In one of the histidines on the $3_{10}$-helix, the $\delta$-nitrogen and the $\varepsilon$-nitrogen have been identified.

as scaffold), and the other consists of the C-$\beta$ atoms and the rest of the imidazole as the side chains. We model these distinct regions using a hybrid approach, with the semiempirical AM1 method applied to the scaffold, and the more accurate B3LYP density functional method employed for imidazole side chains. A proton wire can emerge if hydrogen bonds form between N-donors ($\varepsilon$ nitrogens) and N-acceptors ($\delta$ nitrogens) of the consecutive imidazole moieties from the side chains of histidines. In this work we investigate computationally whether proton wires form from $3_{10}$-, $\alpha$-, and $\pi$-helices, and how the energetics of proton translocation differ among the different helices given the geometrical constraints of these various structures. We also study how helical dipoles can break the symmetry of proton translocation energetics, inducing unidirectional proton motion.

## II. COMPUTATIONAL METHODS

The computational strategy used in this study is based on the hybrid quantum chemistry approach within the ONIOM two-layer formalism.[17−19] The total energy, $E$, was computed as follows:

$$E = E_{\mathrm{low}}(\mathrm{full}) + E_{\mathrm{high}}(\mathrm{subset}) - E_{\mathrm{low}}(\mathrm{subset}) \qquad (1)$$

where $E_{\mathrm{low}}$(full) and $E_{\mathrm{low}}$(subset) are the energies of the full and subset systems, respectively, determined using a relatively inexpensive ("low") computational approach. $E_{\mathrm{high}}$(subset) is the energy of the subset system obtained using a more accurate ("high") model chemistry, in principle providing near-chemical accuracy for the subset of atoms involved in making and breaking bonds. In this study, the full system is the entire peptide, while the subset system consists of the histidine side chains, i.e., the $\beta$ carbons, hydrogen atoms, and the attached imidazole rings. The dangling bonds on $\beta$-carbon were capped with additional hydrogens. Mechanical embedding was used to avoid the problem of overpolarization, i.e., charge distributions on the peptide scaffold were not included in the quantum treatment of side chains.

We employed the AM1 semiempirical molecular orbital method[20] for the "low" level theory; this has been used previously in the study of helical peptides.[21,22] Histidine side chains were treated with B3LYP/6-311G(d,p) as the "high" level of theory.[23−25] We have found that this level of theory/basis set captures hydrogen-bond distances and energies in these systems.[5] Moreover, it has been previously shown that the combination of B3LYP/AM1 gives hydrogen-bond energetics and structures virtually indistinguishable from full DFT applied to peptides.[26]

For each helix, full geometry optimizations were performed for various possible rotamers of the histidines; the one with the lowest energy was reported as the equilibrium structure. Harmonic vibrational analyses were performed to ensure that the optimized structures are at the minima on the potential energy surface. All calculations were performed using Gaussian 03.[27] Initial structures of the peptides were generated by manual superposition with experimentally determined $3_{10}$-, $\alpha$-, and $\pi$-helical structures using visualization in PyMol[28] with peptide rotamers generated using Chimera.[29] For each helix, the *N*-terminus was capped with an acetyl group, while the *C*-terminus was capped with an $NH_2$ group. Figure 1 shows the rotamers that are optimized to the lowest energy structure for each helix. Hydrogen-bond distances were extracted from the optimal rotamers for each helix to investigate the extent of side-chain proton wire formation supported by each helix.

To obtain information on the energetics of proton transfer, a proton was first added to the *N*-acceptor at the end of each wire (H1) followed by a full geometry optimization. The energies of an excess proton at sites H2, H3, etc., were obtained by inducing Grotthuss-shuttling-type motions that localize an excess proton at successive imidazoles along a proton wire. Transition states connecting the various minima of the protonated helices were

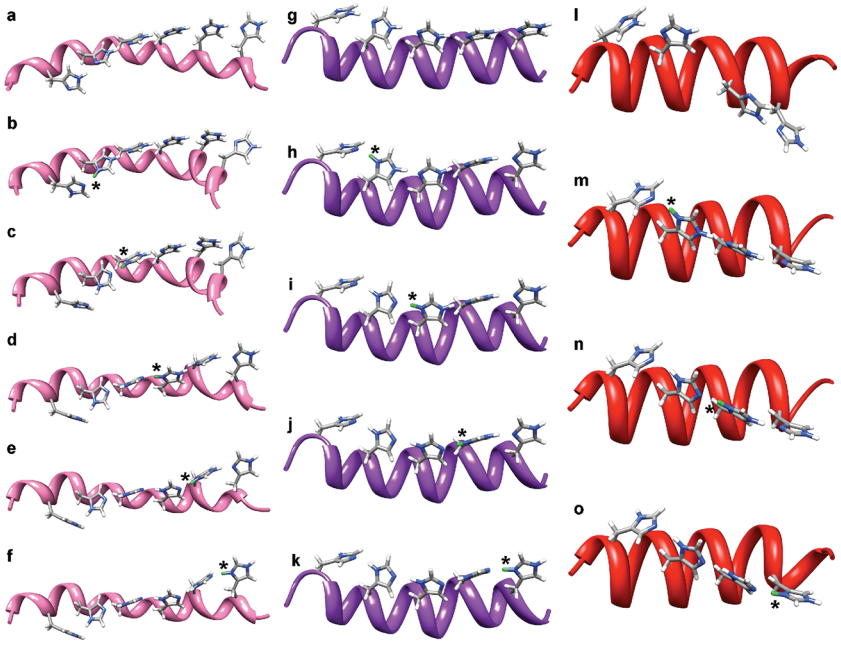


**Figure 2.** Lowest energy equilibrium structures for the $3_{10}$-helix: (a) in the unprotonated state, (b) protonated at $H_2$, (c) protonated at $H_3$, (d) protonated at $H_4$, (e) protonated at $H_5$, and (f) protonated at $H_6$. Lowest energy equilibrium structures for the $\alpha$-helix: (g) in the unprotonated state, (h) protonated at $H_2$, (i) protonated at $H_3$, (j) protonated at $H_4$, and (k) protonated at $H_5$. Lowest energy equilibrium structures for the $\pi$-helix: (l) unprotonated state, (m) protonated at $H_2$, (n) protonated at $H_3$, and (o) protonated at $H_4$. The excess proton is represented as a green bond (and marked with an *) in the equilibrium structure. Proton locations result from optimizations, and may differ markedly from initial conditions.

computed and confirmed by normal-mode analysis at critical points yielding one imaginary vibrational frequency associated with a proton transfer reaction coordinate. These frequencies were found to be in the range of $900i-1600i$ cm$^{-1}$.

Various energetic and structural properties were computed to characterize the protonated systems. The proton affinity (PA > 0) was determined by computing the energy difference between the optimized unprotonated and optimized protonated species. In addition, the desorption energy (DE > 0) was obtained by computing the energy difference between an initial, nonoptimized protonated species and the final, optimized protonated structure. We also computed polypeptide polymerization energies for comparison with results from previous studies[22] and to quantify added stability from proton-wire formation. The capped helices can be viewed as being formed from alanines, histidines, acetic acid, and ammonia following the reaction

$$(21-N)\text{Alanines} + N\text{Histidines} + \text{Acetic Acid} + \text{Ammonia} \rightarrow \text{acetyl}-(\text{ala})_{21-N}(\text{His})_N-\text{NH}_2 + (N+1)\text{Water} \quad (2)$$

where $N$ is the number of histidines in the peptide. For this reaction, the polymerization energy of the peptide can be computed according to

$$\Delta E = E_{\text{Peptide}} + (\text{N}+1)E_{\text{Water}} - E_{\text{Acetic Acid}} - E_{\text{Ammonia}} - (21-N)E_{\text{Alanines}} - NE_{\text{Histidines}} \quad (3)$$

Here $N$ equals 6, 5, and 4 for the $3_{10}$-, $\alpha$-, and $\pi$-helices, respectively. The values of energy for the alanines and histidines were computed by optimizing the geometry of the isolated most stable configurations (without the internal formation of H-bonds) at a B3LYP/6-311G(d,p) level. The same level of optimization was performed for water and acetic acid, whereas, the energy of the peptide was computed by performing a single-point B3LYP/6-311G(d,p) calculation at the ONIOM optimized geometry. For each helix, we computed the polymerization energy for three cases: pure polyalanine, unprotonated polyalanine with histidines substitutions (i.e., proton wires), and protonated proton wires.

Two properties were calculated to quantify structural changes occurring in the peptides during protonation and proton motion from *N*- to *C*-terminus. To quantify gross structural distortions, the root-mean-square deviation (RMSD) between any two structures was computed with respect to the positions of corresponding atoms for any particular region of the peptide. In addition, to assess the bending of the helices, the angle between a particular structure and a reference structure was computed.[30] This angle, termed the local tilt, was obtained using the initial structures (Figure 1) as references. In the calculations of both RMSD and local tilt angle, the two compared structures were aligned with respect to their peptide backbones using VMD software.[31]

## III. RESULTS AND DISCUSSION

The lowest energy structures for the $3_{10}$-, $\alpha$-, and $\pi$-helices in both unprotonated and protonated states are shown in Figure 2. All of these gas-phase structures were found to fold into stable helical conformations that maintain the overall starting helical geometry. To simplify the discussion, imidazoles have been labeled HX where X = 1 through $M$ = total number of histidines for a given helix, with H1 being closest to the N terminus. For the $3_{10}$-, $\alpha$-, and $\pi$-helices, $M$ = 6, 5, and 4, respectively.

In the unprotonated $3_{10}$-helix, all six imidazoles are linked by hydrogen bonds between *N*-donors and *N*-acceptors with an

**Table 1. RMSD Calculated between the Unprotonated and Protonated Equilibrium Structures of the Peptides with Protonation of the Indicated Histidine (His) Residue**

| helix | protonated HIS | RMSD (Å) |
|---|---|---|
| $3_{10}$- | H2 | 2.34 |
| | H3 | 2.39 |
| | H4 | 1.84 |
| | H5 | 2.16 |
| | H6 | 2.17 |
| $\alpha$- | H2 | 0.75 |
| | H3 | 0.65 |
| | H4 | 0.61 |
| | H5 | 0.62 |
| $\pi$- | H2 | 2.06 |
| | H3 | 2.01 |
| | H4 | 0.36 |

average hydrogen-bond distance of 2.00 ± 0.01 Å (Figure 2a), forming a stable, continuous proton wire. The scaffold conserves its helical structure with a local tilt angle of ~3°. RMSDs between the initial structure (Figure 1a) and the lowest energy equilibrium structure (Figure 2a) show considerable changes in both termini (4.3 ± 0.1 Å), and in the alanine adjacent to the *N*-terminus (4.8 ± 0.1 Å). The RMSD of the scaffold is only 2.0 ± 0.3 Å, reflecting a relatively small distortion of the $3_{10}$-helix.

An excess proton was then localized sequentially on each imidazole in the $3_{10}$-helix to investigate the proton energy landscape. When the $3_{10}$-helical peptide was initially protonated at H1, the added proton relaxed to H2, i.e., an H1 protonated state is not observed (Figure 2b). Additional minima were obtained with the proton at H3 (Figure 2c), H4 (Figure 2d), H5 (Figure 2e), and H6 (Figure 2f). RMSDs between adjacent minima ranged from 1.84 to 2.39 Å (Table 1), indicating relatively small changes in peptide structure during proton translocation through the wire. All minima obtained for the protonated $3_{10}$-helix exhibit local tilt angles between 1° and 3°.

Similarly to the stable $3_{10}$-helix, the unprotonated (polyhistidine-substituted) $\alpha$-helix optimized to form a continuous proton wire (Figure 2g). The average hydrogen-bond distance for the wire is 1.98 ± 0.05 Å. As with the $3_{10}$-helix, the $\alpha$-helical scaffold suffers only minor changes—mainly in the termini—with RMSDs ranging from 0.02 to 0.1 Å and a local tilt angle of ~1°. Examination of the protonated structures (Figure 2h−k) shows the same behavior previously discussed for the $3_{10}$-helix, i.e., minima at H2 (Figure 2h), H3 (Figure 2i), H4 (Figure 2j), and H5 (Figure 2k). In this case, RMSD values for adjacent minima, which ranged from 0.62 to 0.75 Å (Table 1), were smaller than in the $3_{10}$-helix.

In contrast to the stable structures of the $3_{10}$- and $\alpha$-helices, the unprotonated polyhistidine-substituted $\pi$-helix forms a discontinuous proton wire (Figure 2l). In particular, H1 and H2 form the first segment of the wire, while H3 and H4 form the second segment. We term this discontinuous wire a (2,2)-wire. The hydrogen-bond distance for both segments is basically the same (1.99 Å). The RMSD values are relatively small, ranging from 1.3 to 1.5 Å (Table 1). Examination of the protonated structures (Figure 2m−o) shows that when H1 is initially protonated, the proton relaxes to H2, and the wire relaxes to a continuous network, and then retains its continuity when the excess charge is localized on H3, and again on H4. The local tilt angle in all cases for the $\pi$-helix was found to be negligible. The RMSD for the protonated structures ranged from 1.5 to 2.4 Å (Table 1).

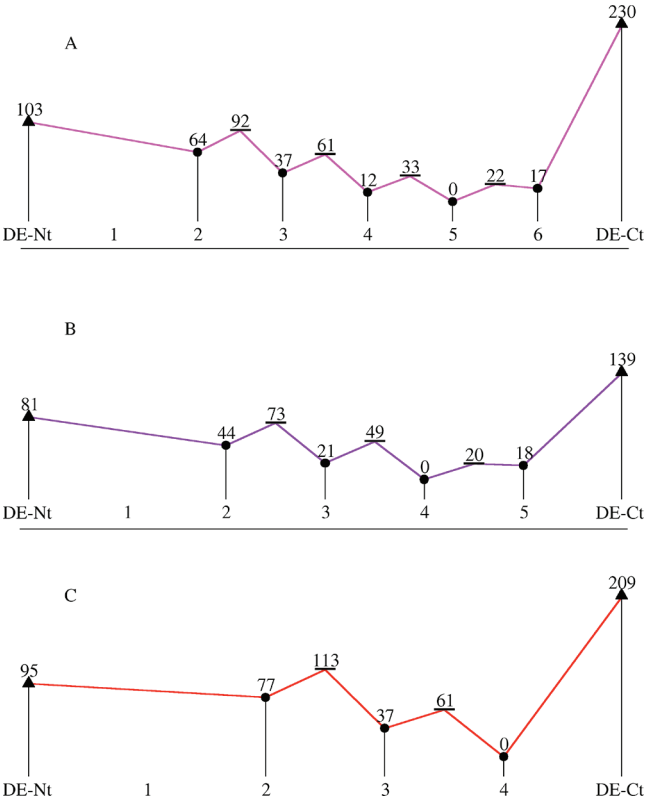


**Figure 3.** Proton translocation potential energy surface for (A) $3_{10}$-helix, (B) $\alpha$-helix, and (C) $\pi$-helix. For each protonated helix, the ground state energy is set to zero.

It is interesting to note that in all cases no minimum was found on the H1 histidine, whereas minima were obtained in the histidine proximal to the *C*-terminus. A plausible explanation for this is the large macroscopic dipole moment of the helices, which induces stabilization of the excess proton in the histidine proximal to the *C*-terminus.

The propensity for these three types of helices to form continuous imidazole wires can be correlated to their vertical spacings, i.e., their histidine repeat distances. In particular, the vertical spacing of the side chains in $3_{10}$- and the $\alpha$-helices, which form continuous wires, is 6.0 Å and 6.6 Å, respectively, whereas the discontinuous wire formed in the $\pi$−helix has a vertical spacing of 7.0 Å. Hence, we can conclude that helical peptides possessing vertical spacings of approximately 6.6 Å or smaller are required to support continuous hydrogen-bonded wires built from imidazole (and triazole) groups. This result is consistent with our previous calculations on proton wires on effective backbones of various lengths.[5] Future research is required to determine whether consistently continuous ($3_{10}$- and $\alpha$-helices) or transient-continuous ($\pi$-helices) proton wire produces faster proton diffusion and conduction.

Our calculations predict that in the lowest energy structure of each helix, the $\varepsilon$-protons on imidazole side chains point toward the *C*-terminus of the peptide. The likely reason for this is that helical peptides have a macrodipole moment, resulting from the cumulative effect of the oriented dipole of each peptide bond.

Table 2. Proton Affinity (PA), Desorption Energy (DE), and Range of Energy Barriers (REB) in kJ/mol for the Three Helices[a]

| helix | PA (kJ/mol) *N*-terminus | PA (kJ/mol) *C*-terminus | DE (kJ/mol) *N*-terminus | DE (kJ/mol) *C*-terminus | REB (kJ/mol) |
|---|---|---|---|---|---|
| $3_{10}$- | 1113 | 1194 | 103 | 230 | 21−28 |
| $\alpha$- | 1110 | 1199 | 81 | 139 | 20−29 |
| $\pi$- | 1108 | 1220 | 95 | 209 | 24−36 |

[a] PA and DE were calculated when the proton was added to either the *N*-terminus or the *C*-terminus.

The amino end (*N*-terminus) of peptide helices supports a partial positive charge, while the carboxyl end (*C*-terminus) contains a partial negative charge, thus the tendency of the proton is to point toward the carboxyl terminus. These results suggest that this helical dipole is sufficient to orient the proton wire toward the negative end of the helical dipole, which may serve as sufficient driving force to bias proton transfer to unidirectional conduction.

To understand the energetics of proton transfer for each helix, the potential energy surface was calculated as a function of the collective proton translocation position (Figure 3). We note that previous ab initio molecular dynamics simulations have shown that the free-energy surface for protons sitting on imidazole-based proton wires retains the same qualitative shape as that of the underlying potential energy surface, with protons embedding into wire interiors occurring spontaneously at ambient temperature.[5] The same is expected in these helical systems because of the relative rigidity of these helices as found above.

For each helix, the energy of the ground state protonated species was set to zero. In all three cases, a slightly lower energy was obtained for excess charge localization closest to the *C*-terminus, because of the partial negative charge on this terminus (see also Table 2). In the case of the $3_{10}$-helix (Figure 3A), the differences in energy between adjacent minima are between 27 kJ/mol (translocation of the proton from H2 to H3) and 12 kJ/mol, and energy barriers are less than 28 kJ/mol. All the energy differences between adjacent minima are "downhill" except for the H5−H6 difference, which is "uphill" by 17 kJ/mol.

In the case of the $\alpha$-helix (Figure 3B), the energy differences between adjacent minima range from 23 to 18 kJ/mol (with an uphill transition between H4 and H5 of 18 kJ/mol), and energy barriers are below 29 kJ/mol. Thus, $3_{10}$- and $\alpha$- helices, which produce consistently continuous proton wires, exhibit very similar proton translocation energetics.

In the case of the $\pi$-helix (Figure 3C), all energy differences between minima are downhill, i.e., difference between H2 and H3 minima is 40 kJ/mol and between H3 and H4 is 37 kJ/mol. The energy barriers are 36 and 24 kJ/mol. These results suggest that the polyhistidine-substituted $\pi$-helix behaves quite differently from $3_{10}$- and $\alpha$-helices in wire continuity, energy landscape shape, and, to some extent, barriers heights.

Proton affinities (PA) and desorption energies (DE) were calculated at the *N*- and *C*-termini of each helix (Figure 3, Table 2). In all cases, the PA is higher for protonation of the histidine closest to the *C*-terminus—by as much as 112 kJ/mol for the $\pi$-helix—because of helical-dipole stabilization. The PA is largest for the $\pi$-helix, followed by the $\alpha$-helix, and finally the $3_{10}$-helix. This same ordering is observed for the magnitude of the helical dipole moment: 33.7 D, 55.7 D, and 69.9 D for the $\pi$-, $\alpha$-, and $3_{10}$-helices, respectively. We note that PA values correlate with RMSD values between initial, unprotonated structures and protonated H1 structures. On the other hand, desorption energies, which are a measure of stabilization as excess charge embeds from the end to the heart of the wire, were not found to correlate with RMSDs, and give a different ordering with respect to helices ($3_{10}$-helix > $\pi$-helix > $\alpha$-helix). All desorption energies were found to be higher for charge localization on H6 (proximal to the *C*-termini), again from helical-dipole stabilization.

Table 3. Polymerization Energies in kJ/mol for the Three Helices, Each in Three States: Unprotonated Pure Polyalanines ($\Delta E^{U}_{Polyala}$), Substituted with Histidines (i.e., Proton Wires) but Unprotonated ($\Delta E^{U}_{His\text{-}substituted}$), and Protonated Proton Wires ($\Delta E^{P}_{His\text{-}substituted}$)

| helix | $\Delta E^{U}_{Polyala}$ (kJ/mol) | $\Delta E^{U}_{His\text{-}substituted}$ (kJ/mol) | $\Delta E^{P}_{His-substituted}$ (kJ/mol) |
|---|---|---|---|
| $3_{10}$- | −72 | −127 | −1230 |
| $\alpha$- | −61 | −201 | −1259 |
| $\pi$- | −42 | −90 | −1112 |

The polymerization energy for each helix was calculated and used as a measurement of the stability of each proton wire. Table 3 shows polymerization energies for the three helices, each in three states: unprotonated pure polyalanines, substituted with histidines (i.e., proton wires) but unprotonated, and protonated proton wires. Polymerization is predicted to be exoergic in all cases, but with a considerable increase in stability upon protonation because of the assumption of a gas-phase proton reference state. For the pure polyalanines peptides, we observed that the $3_{10}$-helix is the most stable system, followed by the $\alpha$-helix, and finally the $\pi$-helix. These results are in agreement with ref 22, which predicted that $3_{10}$-helical polyalanines peptides are slightly more stable than similar peptides with $\alpha$-helical structure due to the optimal alignment of backbone hydrogen bonds driving helix formation. In the case of the unprotonated proton wires, the $\alpha$-helix is the most stable system, followed by the $3_{10}$-helix, and finally the $\pi$-helix. When comparing the results of the pure polyalanines peptides with the histidine-substituted peptides, we observed that the $\alpha$-helix is stabilized by 141 kJ/mol, the $3_{10}$-helix by 55 kJ/mol, and the $\pi$−-helix by 48 kJ/mol. Hence, it is clear that the formation of the proton wire increases the stability of the peptide considerably, especially for the $\alpha$-helix. Upon protonation of histidine substituted peptides, all helices are considerably more stable, thus conserving the same stability ordering observed for the unprotonated wires.

## IV. CONCLUDING REMARKS

In summary, accurate electronic structure methods predict that an imidazole-based proton wire can form from histidine-containing helical peptides. Our calculations suggest that substituted $3_{10}$- and $\alpha$-helices can translocate protons in vacuum with relatively rapid kinetics compared to those of the $\pi$-helix. The $\pi$-helix exhibits both continuous and discontinuous proton wires, for protonated and unprotonated states, respectively. What is most striking is the prediction that helical dipoles can

bias the position of an excess proton toward the C-terminus, by as much as 112 kJ/mol in our calculations. Our calculations also predict that $\alpha$-helices are the more stable compared to $3_{10}$- and the $\pi$−helices due to better alignment of imidazole groups. In forthcoming work we will report on dynamics calculations on these systems, as well as peptide synthesis and characterization to test these predictions.

## AUTHOR INFORMATION

### Corresponding Author

*E-mail: gustavo.lopez@upr.edu or gustavo.lopez1@lehman.cuny.edu.

## ACKNOWLEDGMENT

We acknowledge funding from the National Science Foundation Center for Chemical Innovation Program (CHE-0739227) and CURE-REU program (CHE-1004983). We thank all members of the UMass Fueling the Future Center for Chemical Innovation for stimulating discussions on charge transfer. SMA thanks Prof. Horia Metiu and the UCSB Department of Chemistry for providing an ideal environment for study.

## REFERENCES

(1) Bai, H.; Winston Ho, W. S. *Polym. Int.* **2010**, *60*, 26–41.
(2) Woudenberg, R. C.; Yavuzcetin, O.; Tuominen, M. T.; Coughlin, E. B. *Solid State Ionics* **2007**, *178*, 1135–1141.
(3) Ojemyr, L.; Sanden, T.; Widengren, J.; Brzezinski, P. *Biochemistry* **2009**, *48*, 2173–2179.
(4) Vijayvergiya, V.; Wilson, R.; Chorak, A.; Gao, P. F.; Cross, T. A.; Busath, D. D. *Biophys. J.* **2004**, *87*, 1697–1704.
(5) Viswanathan, U.; Basak, D.; Venkataraman, D.; Fermann, J. T.; Auerbach, S. M. *J. Phys. Chem. A.* **2011**, *115*, 5423–5434.
(6) Marqusee, S.; Robbins, V. H.; Baldwin, R. L. *Proc. Natl. Acad. Sci. U.S.A.* **1989**, *86*, 5286–5290.
(7) Scholtz, J. M.; Marqusee, S.; Baldwin, R. L.; York, E. J.; Stewart, J. M.; Santoro, M.; Bolen, D. W. *Proc. Natl. Acad. Sci. U.S.A.* **1991**, *88*, 2854–2858.
(8) Levy, Y.; Jortner, J.; Becker, O. M. *Proc. Natl. Acad. Sci. U.S.A.* **2001**, *98*, 2188–2193.
(9) Nguyen, H. D.; Marchut, A. J.; Hall, C. K. *Protein Sci.* **2004**, *13*, 2909–2924.
(10) Sezer, D.; Freed, J. H.; Roux, B. *J. Phys. Chem. B* **2008**, *112*, 5755–5767.
(11) Oommachen, S.; Ren, J; McCallum, C. M. *J. Phys. Chem. B* **2008**, *112*, 5702–5709.
(12) Salvador, P.; Asensio, A.; Dannenberg, J. *J. Phys. Chem. B* **2007**, *111*, 7462–7466.
(13) Job, G. E.; Kennedy, R. J.; Hitmann, B.; Miller, J. S.; Walker, S.; Kemp., D. S. *J. Am. Chem. Soc.* **2006**, *128*, 8227–8233.
(14) Kennedy, R. J.; Sharon, S. M.; Kemp, D. S. *J. Am. Chem. Soc.* **2005**, *127*, 16961–16968.
(15) Wieczorek, R.; Dannenberg, J. J. *J. Am. Chem. Soc.* **2003**, *125*, 8124–8129.
(16) Morozov, A. V; Tsemekhman, K.; Baker, D. *J. Phys. Chem. B* **2006**, *110*, 4503–4505.
(17) Vreven, T.; Morokuma, K. *J. Comput. Chem.* **2000**, *21*, 1419–1432.
(18) Vreven, T.; Morokuma, K; Farkas, O.; Schlegel, H. B.; Frisch, M. J. *J. Comput. Chem.* **2003**, *24*, 760–769.
(19) Vreven, T.; Byun, K. S.; Komaromi, I.; Dapprich, S.; Montgomery, J. A.; Morokuma, K.; Frisch, M. J. *J. Chem. Theory Comput.* **2006**, *2*, 815–826.
(20) Dewar, M. J. S.; Zoebisch, E. G.; Healy, E. F.; Steward, J. J. P. *J. Am. Chem. Soc.* **1985**, *107*, 3902–3909.
(21) Wieczorek, R.; Dannenberg, J. J. *J. Am. Chem. Soc.* **2004**, *126*, 12278–12279.
(22) Wieczorek, R.; Dannenberg, J. J. *J. Am. Chem. Soc.* **2004**, *126*, 14198–14205.
(23) Becke, A. D. *J. Chem. Phys.* **1993**, *98*, 5648–5653.
(24) Lee, C.; Yang, W.; Parr, R. G. *Phys. Rev. B* **1998**, *37*, 785–789.
(25) Krishman, R.; Binkley, J. S.; Seeger, R.; Pople, J. *J. Chem. Phys.* **1980**, *72*, 650–655.
(26) Plumley, J. A.; Dannenberg, J. J. *J. Phys. Chem. B* **2011**, *115*, 10560–10566.
(27) Frisch, M. J.; Trucks, G. W.; Schlegel, H. B.; Scuseria, G. E.; Robb, M. A.; Cheeseman, J. R.; Montgomery, Jr., J. A.; Vreven, T.; Kudin, K. N.; Burant, J. C. et al. *Gaussian 03*, revision C.02; Gaussian, Inc.: Wallingford CT, 2004.
(28) DeLano, W. L. *The PyMOL Molecular Graphics System*; DeLano Scientific LLC: Palo Alto, CA, 2008; http://www.pymol.org.
(29) Pettersen, E. F.; Goddard, T. D.; Huang, C. C.; Couch, G. S.; Greenblatt, D. M.; Meng, E. C.; Ferrin, T. E. *J. Comput. Chem.* **2004**, *25*, 1605–1612.
(30) Mezei, M.; Filizola, M. *J. Comput.-Aided Mol. Des.* **2006**, *20*, 97–107.
(31) Humphrey, W.; Dalke, A.; Schulten, K. *J. Mol. Graphics* **1996**, *14*, 33–38.